# Research of the LDA Calibration Facility's Uncertainty

J. Lu*, B. Mickan, W. Shu, N. Kurihara, D. Dopheide
Physikalisch-Technische Bundesanstalt(PTB), Germany

**Abstract.** The paper presents an investigation on the uncertainty of calibration facility for LDA. It discusses the each uncertainty source of the facility. A novel approach is applied to assess dynamically the uncertainty of the rotating disc's roundness deviation. With this method, we have the relative expanded uncertainty as $U_{95}=5.5\times10^{-4}$ for 95% confidence about the facility.

**Key words** LDA calibration facility uncertainty evaluation

## 1. Introduction

The measurement of flow velocity $u_o$ with LDA can be ascertained [1] as

$$u_o = S \cdot f_D = \frac{\lambda}{2 \cdot \sin\frac{\varphi}{2}} \cdot f_D \qquad (1)$$

where $f_D$ is the Doppler frequency, S the fringes spacing, or say the instrument constant, $\lambda$ the wavelength of laser beam, and $\varphi$ the angle between two laser beams. The task of the LDA calibration focuses on determining S, which is ascertained in most calibration laboratories by measuring LDA's $f_D$ with the known $u_o$. There exist several different ways to generate the constant particle velocity $u_o$. A method widely used is based on the rotating disc. Physikalisch - Technische Bundesanstalt (PTB) set up such a calibration facility several years ago[2]. The purpose of this paper is to investigate the uncertainty of the facility, which enjoys an important position in LDA calibration.

## 2. LDA calibration facility

Fig. 1 is the schematic diagram about this facility, which is composed of following parts: the rotating disc and its driving mechanism, the individual particle choosing device and LDA signal acquisition and processing unit as well as the numerical controlled transverse.

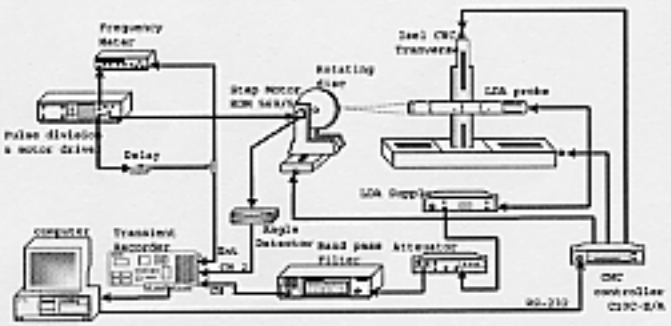


Fig. 1 The schematic diagram of LDA calibration facility

The rotating disc of the facility is cylindroid in shape, with about 15 mm cylindrical height . The disc is made up with transparent glass, its mean radius r = 92.0787 mm, the maximal eccentricity is less than 7 μm determined by coordinator measuring machines. A step motor is used to drive the disc so its rotating angular frequency ω is controllable. The tangent velocity of the particles on the cylindrical surface of the disc will be:

$$u_t = r \cdot \omega \qquad (2)$$

Two coherent laser beams are crossed and focused on the cylindrical surface of the disc to form an ellipsoidal measuring volume consisting of interference fringes. As the particles on the cylindrical surface pass through the fringes during the rotation of the disc , the scattering signal of the particles will be picked up by the photodiode of LDA. It renders the tangent velocity of these particles. Fig.2 shows the relation between the scattering particle on the rotating disc and measuring volume. In this case, the tangent velocity of a particle will be orthogonal to the fringes.

It is important for the driving mechanism to keep the rotating disc moving in constant angular frequency. This driving mechanism consists of a pulse generator, a step motor, a rotating angle detector and a frequency meter. The frequency meter is used to get the periods of the disc revolution and delayed pulses to locate the relative circumferential position of the particle to be measured. In addition, it can monitor the constancy of the angular frequency.

There are some cases of overlapped scattering particles in the measuring volume. The multi-particles will cause fluctuation of $f_D$ signal. A device is needed to choose the individual particle by conjugation of a logic- gate-selecting signal and trigger signal at signal sampling. By tuning the phase of the delayed AND pulse used as the external trigger signal, a satisfactory Doppler burst of individual particle can be obtained.

## 3. Uncertainties sources due to installation

If there were no installations error, the uncertainty analysis would be based simply upon:

$$S = \frac{\omega \cdot r}{f_D} \qquad (3)$$

(* present address: China Institute of Metrology,
Hangzhou 310034, P.R.China, lvjin@telekbird.com.cn)

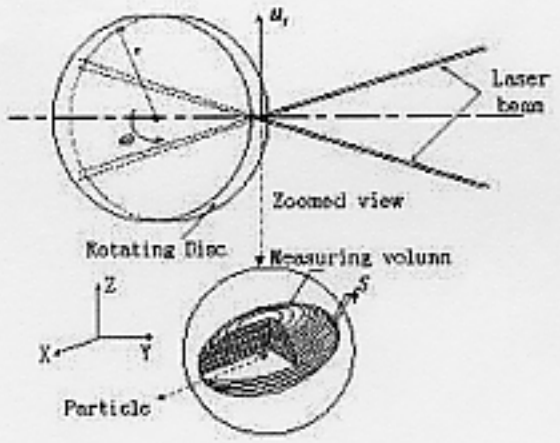


Fig. 2 The relation between the scattering particle on the rotating disc and measuring volume

In practice, the installation error is unavoidable. There are two practical possibilities:

1) The altitude of LDA probe in Z axis direction is not the same as that of the disc's center, i.e. the light axis of LDA is not through the center of rotating disc. In this case, the measuring volume position is changed up or down from the normal position, as shown in Fig 3 (a) from P to P'. Consequently, an error will occur about the tangent velocity $u_t$, because $u_t$ is not exactly the transversal velocity across the fringes. The actual velocity to be measured will be the velocity projection orthogonal to the fringes $u_{o1}$, i.e.

$$u_{o1} = u_t \cdot \cos\alpha \qquad (4)$$

where $\alpha$ is the inclination angle between the normal line of the fringes and tangent line at P' position.

In practical calibration, it is attempted to avoid this case by ensuring the speckles symmetry of incident and scattering beams to adjust the altitude of the probe in Z axis direction. When the altitude of LDA probe in X axis direction is lower than the height of the rotating disc's center, the direction of normal line n' of scattering will rotate with $\alpha$, the asymmetric speckles of incident and scattering beams occur as shown in Fig 3(b), where I and I' represent the two speckles of incident beams, and R as well as R' represents the two speckles of scattering beams. L is the distance between the LDA's lens and the rotating disc rim, L is about 300mm.

2) The rotating disc may have a position deflection shown as Fig. 4. In this way, the velocity magnitude to be measured will be the vertical projection of the tangent velocity of the disc $u_t$. It is the same occasion as that of the improper installation of the calibrated LDA probe so that the plane of the transmitting beams h as an obliquity to the disc plane while the disc is in perfectly installation position.

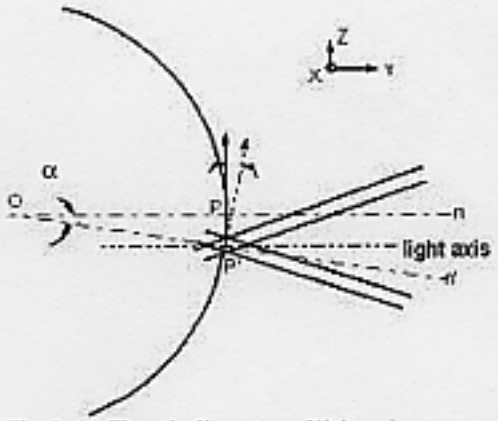


Fig. 3 (a) The misalignment of light axis

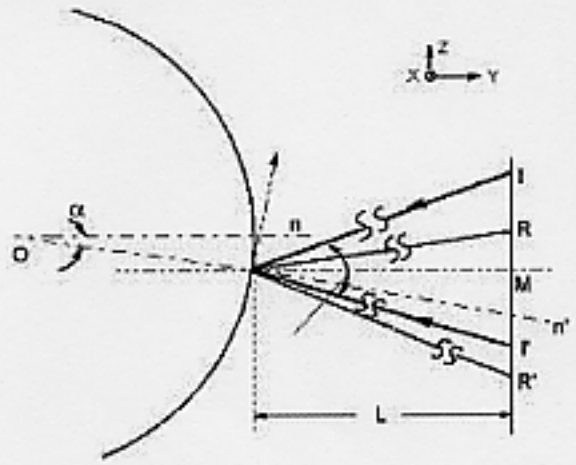


(b) Asymmetric speckles of incident and scattering beams

Assuming that the obliquity is $\beta$, the measured velocity projection in Z-axis $u_{o2}$ will be:

$$u_{o2} = u_t \cdot \cos\beta \qquad (5)$$

The positional relation between the error sources $\alpha$ and $\beta$ discussed above can be illustrated by Fig.5, and (4) should be modified as

$$S = \frac{\omega \cdot r}{f_D} \cdot \cos\alpha \cdot \cos\beta \qquad (6)$$

This is a typical "cosine error" problem, which have been expatiated in Annex F of [3]. By [3], two new variables $\delta_1$=1-cos $\alpha$ and $\delta_2$=1-cos $\beta$ can be introduced, assuming $\alpha \approx 0, \beta \approx 0$, or $\delta_1 << 1, \delta_2 << 1$ as is the case in practice. Then we have

$$S = \frac{r \cdot \omega}{f_D} \cdot (1-\delta_1) \cdot (1-\delta_2) \approx \frac{r \cdot \omega}{f_D} \cdot (1-\delta_1-\delta_2) \qquad (7)$$

where $\delta_1 \approx \alpha^2/2$, $\delta_2 \approx \beta^2/2$ .

Following is the discussion about the uncertainty for every item in (7) in detail.

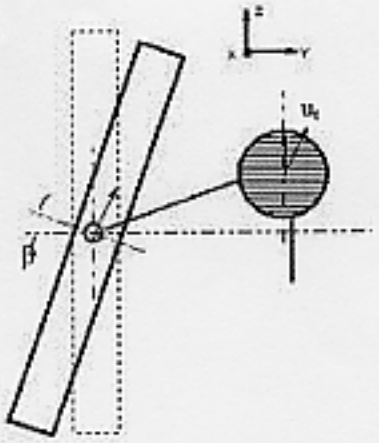

Fig. 4 Inclination angle of the disc

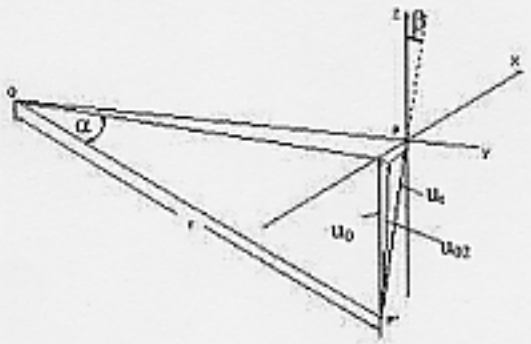

Fig. 5 The positional relation between α and β

## 4. Uncertainty estimation

By derivation of (7), the uncertainty analysis expression about S can be written as

$$u_c^2(S)/S^2 = c_r^2 u^2(r) + c_\omega^2 u^2(\omega) + c_{f_D}^2 u^2(f_D) + c_{\delta_1}^2 u^2(\delta_1) + c_{\delta_2}^2 u^2(\delta_2) \quad (8)$$

with the sensitivity coefficients as follows,

$$c_r = \frac{\partial S}{\partial r}\cdot\frac{1}{S} \approx \frac{\omega}{f_D}\cdot(1-\delta_1-\delta_2)\cdot\frac{1}{S} = \frac{1}{r} \quad (8.1)$$

$$c_\omega = \frac{\partial S}{\partial \omega}\cdot\frac{1}{S} \approx \frac{r}{f_D}\cdot(1-\delta_1-\delta_2)\cdot\frac{1}{S} = \frac{1}{\omega} \quad (8.2)$$

$$c_{f_D} = \frac{\partial S}{\partial f_D}\cdot\frac{1}{S} = -\frac{r\cdot\omega}{f_D^2}\cdot(1-\delta_1-\delta_2)\cdot\frac{1}{S} = -\frac{1}{f_D} \quad (8.3)$$

$$c_{\delta_1} = \frac{\partial S}{\partial \delta_1}\cdot\frac{1}{S} = -\frac{r\cdot\omega}{f_D}\cdot\frac{1}{S} = \frac{1}{(1-\delta_1-\delta_2)} \quad (8.4)$$

$$c_{\delta_2} = \frac{\partial S}{\partial \delta_2}\cdot\frac{1}{S} = -\frac{r\cdot\omega}{f_D}\cdot\frac{1}{S} = \frac{1}{(1-\delta_1-\delta_2)} \quad (8.5)$$

If it is noted as $K=(1-\delta_1-\delta_2)$, then (10) can be modified as

$$\frac{u_c^2(S)}{S^2} = \left(\frac{u(r)}{r}\right)^2 + \left(\frac{u(\omega)}{\omega}\right)^2 + \left(\frac{u(f_D)}{f_D}\right)^2 + \frac{u(\delta_1)^2}{K^2} + \frac{u(\delta_2)^2}{K^2} \quad (9)$$

Each contributory item in this expression is analyzed as follows.

### 4.1. $\delta_1$ and $\delta_2$

When the laser light axis is through the center of rotating disc (Fig 3(b)), the relations about the scattering speckles position and beams are

$$\overline{MR} = \overline{M'R'} \qquad and \qquad tg\frac{\varphi}{2} = \frac{\overline{IM}}{L}.$$

Thus it is expected to keep $\overline{IR} = \overline{I'R'}$ as far as possible in calibration practice.

In the case of the laser light axis being misaligned, it leads $\overline{MR} \neq \overline{M'R'}$ for the scattering speckles. Let the asymmetric value be defined as
$Asym=(\overline{IR} - \overline{I'R'})/2$, it will approximate as following as long as α being small.

$$A_{sym} \approx L\cdot tg\alpha \approx L\cdot\alpha$$

*Asym* can be kept in 1mm, then it yields

$$\alpha = \frac{A_{sym}}{L} = \frac{1}{300} \approx 0.0033 \quad rad$$

α is satisfactory with the symmetric rectangular distribution about its expected value of zero within the bound of 0.0033 rad, or ± 0.00165 rad. By [3], it has

$$E(\delta_1) = \frac{0.00165^2}{6} = 4.537\times10^{-7} \text{ rad}$$

$$u(\delta_1) = \sqrt{\frac{0.00165^4}{45}} = 4.058\times10^{-7} \text{ rad.}$$

The obliquity β is also expected to be a symmetric rectangular distribution with upper and lower bounds of +0.5° and -0.5°, or $-0.0087 \le \beta \le 0.0087$ rad. Similarly, we have

$$E(\delta_2) = \frac{0.0087^2}{6} = 1.26\times10^{-5} \quad rad$$

$$u(\delta_2) = \sqrt{\frac{0.0087^4}{45}} = 1.128\times10^{-5} \quad rad$$

### 4.2. ω

The angular frequency ω of the rotating disc is expected to be kept in constant during the calibration. By formula $\omega=2\pi\cdot f=2\pi / T$, where T is the periodic pulses of the rotating disc, we have the uncertainty expression of ω as

$$u(\omega) = 2\pi\cdot\frac{-u(T)}{T^2} \quad (9)$$

According to the record of the disc's periodic pulses, we have :

Mean of T: 100015.06897

Standard Deviation of T: 17.736

The fluctuation of periodic pulses is met with the Gaussian distribution, the standard deviation of the fluctuation of periodic pulses can be taken as the standard uncertainty. Therefore the uncertainty of the angular frequency can be yielded as follows

$$u(\omega) = 2\pi\cdot\frac{-u(T)}{T^2} = -\frac{2\pi\cdot17.736}{\cdots\cdots^2} \approx 1.114\times10^{-8} \quad rad$$

### 4.3. r

The disc radius r is the major factor for the tangent velocity determination. Uncertainty of r in dynamic state will be different from that of static one due to the high angular frequency of the disc, the influence of its roundness, its mass inhomogeneity and driving machinery assembly. We can known as the static and dynamic roundness uncertainty respectively. The static roundness uncertainty is less than $\pm 7\times10^{-5}$ according to the mean radius r and the maximal eccentricity. While the dynamic roundness uncertainty is not easy to be determined. Here a novel approach for determining the r's uncertainty has been applied by means of LDA measurement. By LDA theory, the burst amplitude profile in cross-section of the measuring volume defers to the Gaussian distribution both in the YOZ and XOZ planes as Fig. 6. The maximal burst amplitude should correspond to the center of measuring volume, which reflect r where its scattering particle located. The center points of measuring volume for different particles distributed around the disc form the dynamic circle of the disc. The more the number of the center, the better the dynamic roundness estimation.

Table 1 is a group of measured and fitted results. Fig. 7 is the correspondent dynamic circle of the disc.

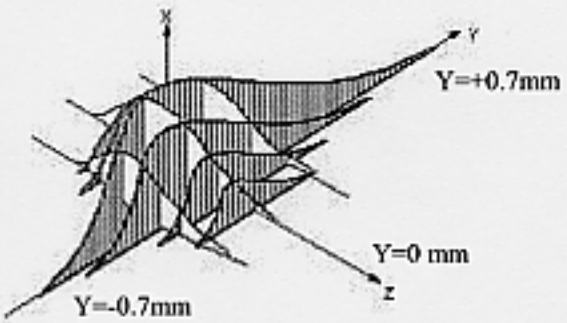


Fig. 6 The burst signal amplitude profiles

Table 1 Dynamic radius measured and fitted results

| No | θ (°) | Δr (mm) | $\chi^2$ | r (mm) |
|---|---|---|---|---|
| 1 | 15.84 | 0.01334 | 0.47911 | 92.09204 |
| 2 | 29.88 | 0.02858 | 0.67253 | 92.10728 |
| 3 | 36 | 0.01533 | 1.09884 | 92.09403 |
| 4 | 52.2 | -2.6E-4 | 0.86286 | 92.07844 |
| 5 | 80.28 | -0.01766 | 1.11836 | 92.06104 |
| 6 | 96.12 | 8.6E-4 | 1.20907 | 92.07956 |
| 7 | 103.32 | -0.04391 | 1.40234 | 92.03479 |
| 8 | 117.72 | -0.02408 | 1.22733 | 92.05462 |
| 9 | 128.16 | -0.01207 | 0.8774 | 92.06663 |
| 10 | 142.56 | -0.00766 | 1.59688 | 92.07104 |
| 11 | 151.92 | -0.01277 | 1.82734 | 92.06593 |
| 12 | 168.12 | -0.01421 | 1.50225 | 92.06449 |
| 13 | 183.24 | -0.0066 | 1.84269 | 92.0721 |
| 14 | 191.16 | 0.02822 | 1.65387 | 92.10692 |
| 15 | 203.04 | -0.00324 | 1.52257 | 92.07546 |
| 16 | 212.4 | -0.00933 | 2.31472 | 92.06937 |
| 17 | 222.84 | 0.0165 | 1.78552 | 92.0952 |
| 18 | 231.48 | 0.02672 | 1.24796 | 92.10542 |
| 19 | 240.48 | 0.0105 | 2.21625 | 92.0892 |
| 20 | 250.2 | -0.00748 | 0.77151 | 92.07122 |
| 21 | 262.8 | 0.00594 | 2.78744 | 92.08464 |
| 22 | 275.04 | -0.00126 | 2.10653 | 92.07744 |
| 23 | 283.68 | 0.03805 | 1.5409 | 92.11675 |
| 24 | 295.92 | 0.0159 | 1.81947 | 92.0946 |
| 25 | 307.8 | 0.00892 | 2.14797 | 92.08762 |
| 26 | 322.92 | 0.01963 | 1.91977 | 92.09833 |
| 27 | 335.88 | -0.01075 | 1.07942 | 92.06795 |
| 28 | 348.48 | -0.03246 | 0.86837 | 92.04624 |
| 29 | 360 | -0.02479 | 1.85205 | 92.05391 |

where θ: the circumferential position of particle; Δr: radius deviation; r: dynamic radius estimate.

An amplitude histogram can be drawn according to the dynamic radius deviation along the circumferential distribution, which is consistent with the Gaussian distribution . The standard deviation of the Gaussian distribution for the histogram represents the uncertainty of the dynamic roundness deviation. Thus we have the uncertainty of the dynamic roundness deviation as :

$$u(r) = \sigma_r = 0.01873(mm)$$

The experiments also show that the dynamic roundness uncertainty is independent of the angular frequency magnitude.

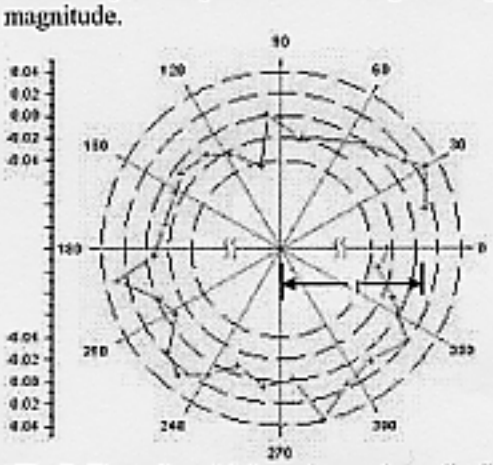


Fig. 7 Circumferential dynamic roundness distribution

### 4.4. $f_D$

The best estimation of $f_D$ can be attained by Cramér-Rao lower bound (CRB) [4-5]. The analytic expression of CRB by [4] has been adopted for decades to find the lower bound of $f_D$ estimation, although there is a difference between the condition of single tone sine signal and Doppler burst, the later has an additional exponential item. According to the analytic expression given by [4-5], the CRB expression for $f_D$ is as

$$\mathrm{var}(f_D) = \frac{6}{(2\pi)^2 \cdot SNR \cdot N \cdot (N^2-1)} \cdot f_s^2 \qquad (11)$$

where $f_S$ is the sampling frequency, SNR the signal to noise ratio, which is defined as $SNR=A^2/2\sigma^2$, A the

Doppler burst amplitude, $\sigma$ the RMS of the noise. In our case, we have the sampling points for each burst N=1024, sampling frequency $f_s=20\times10^6$ Hz, SNR=32 dB or $A^2/2\sigma^2=1584.89$, $f_D=1.15\times10^6$, then

$$u(f_D)=\sqrt{\frac{6\cdot2^2\cdot10^{14}}{(2\pi)^2\cdot1584.89\cdot1024(1024^2-1)}}=5.977 \quad Hz$$

The CRB are almost met by ML estimators when SNR is high. With the simulation results about the performance of ML and FFT estimators in [4], the frequency estimation uncertainty of FFT and ML are not over an order of magnitude. Then it can take the 10 times error bound to the FFT algorithm, i.e. $u(f_D)/f_D = 5.2\times10^{-5}$.

## 5. Uncertainty combination

Table 2 is the list of each contributed uncertainty sources. Each items in Table 3 are independent each other. The combined standard uncertainty $u_c(S)$ can be calculated from (10) by substituting the expectation of the individual terms into (9.1)~(9.5), notice that $K^2=(1-E(\bullet_1)-E(\bullet_2))^2=1$, where $E(\bullet_1)$ and $E(\bullet_2)$ are the expectation of $\bullet_1$ and $\bullet_2$ respectively,

We have: $u_c(S)/S = 2.75\times10^{-4}$.

Table 2 Contributory uncertainty sources list

| Items | Uncertainty Sources | Value | Type | d.o.f. |
|---|---|---|---|---|
| $u(\delta_1)$ | 1. the misalignment of light axis | $4.058\times10^{-7}$ (rad) | B | $\infty$ |
| $u(\delta_2)$ | 2. the inclination angle of the rotating disc | $1.128\times10^{-5}$ (rad) | B | $\infty$ |
| $u(\omega)$ | 3. stability of angular frequency | $1.114\times10^{-8}$ (rad) | A | 28 |
| $u(r)$ | 4. roundness deviation of rotating disc | $1.873\times10^{-2}$ (mm) | A | 28 |
| $u(f_D)$ | 5. frequency estimation | 5.977 (Hz) | B | $\infty$ |

* d.o.f. ---Degrees of freedom

The effective degrees of freedom is calculated according to the Welch-Satterthwaite formula as:

$$df_R=593$$

Since $t_{95}(59) = 2.01$[3], the relative expanded uncertainty for this confidence level is

$U_{95}=2.01\times2.75\times10^{-4}=5.5\times10^{-4}$.

Table 3 shows the occupying factor for each contributory item. It can be seen that the influence of r and $\omega$ uncertainties play a major role in the total variances, while the contributory variances of the inclination angles $\delta_1$ and $\delta_2$ are nearly negligible.

Table 3 The contributory items list

| No | Contributory variances | Value | Occupying percentage |
|---|---|---|---|
| 1 | $U^2(r)/r^2$ | $4.138\times10^{-8}$ | 54.7 % |
| 2 | $u^2(\omega)/\omega^2$ | $3.144\times10^{-8}$ | 41.6 % |
| 3 | $u^2(f_D)/f_D^2$ | $2.7\times10^{-9}$ | 3.6 % |
| 4 | $u^2(\delta_1)/K^2$ | $1.65\times10^{-13}$ | 0.00022 % |
| 5 | $u^2(\delta_2)/K^2$ | $1.27\times10^{-10}$ | 0.0168 % |
| Total variances | | $7.56\times10^{-8}$ | 100 |

## 6. Conclusions

In all uncertainty items to be assessed above, the dynamic roundness uncertainty is the most difficult one to be determined. The novel approach for assessing the uncertainty of the disc's roundness deviation is very effective, it has no relation with the angular frequency magnitude. The dynamic roundness uncertainty is one order greater than the static one.

## References


[1] Durst F, Melling A, Whitelaw J H. Principle and Practice of Laser Doppler Anemometry (2nd Edition)•Academic Press, 1981

[2] Dopheide D: "Neue Halbleitermessverfahren fuer Komplexe Stroemungen", Habilitationsschrift in Universitaet-Gesamthochschule Siegen, Mai 1995

[3] International Standards Organization (ISO), "Guide to the Expression of Uncertainty in Measurement", 1993

[4] Rife D.C. and Boorstyn R.B., "Single tone parameter estimation from discrete time observations", IEEE Trans. Inform. Theory, Vol 20, No. 5, pp 591-598, Sept. 1974

[5] Wriedt T., Bauckhage K.A. and Schoene A., "Application of Fourier Analysis to Phase-Doppler-Signal Generated by Rough Metal Particles", IEEE Tran. on Instru. and Meas., Vol. 38, No.5, Oct.1989, pp.984 -99